Momentum correction for e1f data

M.Mirazita

March 8, 2010

Istituto Nazionale di Fisica Nucleare, Laboratori Nazionali di Frascati, PO 13, 00044 Frascati, Italy

1 Introduction

The momentum correction calculation for the $e1f$ data set is described here, basically following the method applied in the analysis of the π^0 electroproduction [1].

In the first step of the calculation, elastic ep events are used to calculate angle correction. Then, radiative Bethe-Heitler events, together with the unradiated ones, are used to correct the modulus of the electron momentum. These corrections have then been found to work well also for other negative particles.

In a second step, $e\pi^+(n)$ events have been used to calculate π^+ momentum corrections. These last corrections can be satisfactorily used for all the positive particles.

2 Electron-proton event selection

We used the un-skimmed root files [2] of the latest $e1f$ data cooking. The selection of one electron and one proton detected in CLAS is done using the standard SEB particle identification. For the proton and pion, energy loss correction is applied with the *eloss* package modified [3] to take into account the $e1f$ target geometry.

2.1 Coplanarity cut

The basic assumption in the calculation is that photon radiation in the initial (Fig. 1(a)) or the final (Fig. 1(b)) state doesn't change the angle of the radiating electron, so that the detected electron and proton 3-vectors must lay on the same plane, for both radiated and unradiated events.

The azimuthal angle difference

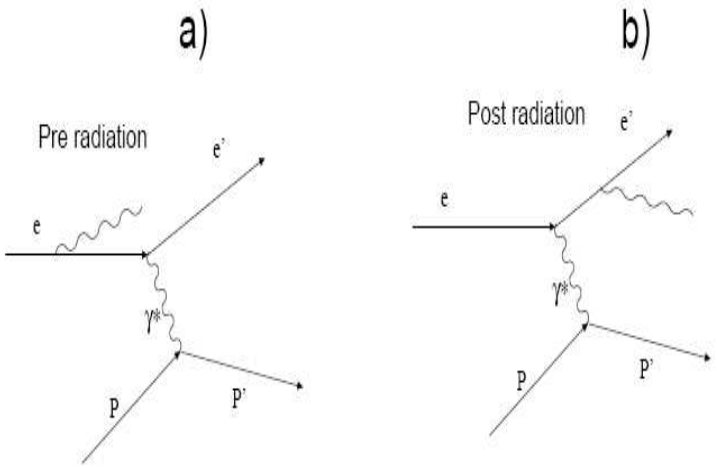

Figure 1: *Bethe-Heitler events with radiation in the initial (a) or final (b) state.*

$$\Delta\phi = |\phi(e) - \phi(p)| \tag{1}$$

is shown in the the Fig. 2 in 23 W-bins between 0.8 and 3.1 GeV, 0.1 GeV wide. Each distribution has been fitted with a gaussian peak plus a second order polynomial. The plot in Fig. 3 shows the mean values (with the error bars representing 3 σ) from the fits of the distributions. Since no W dependence has been found, the cut

$$|\Delta\phi - \pi| < 2^o \tag{2}$$

has been used.

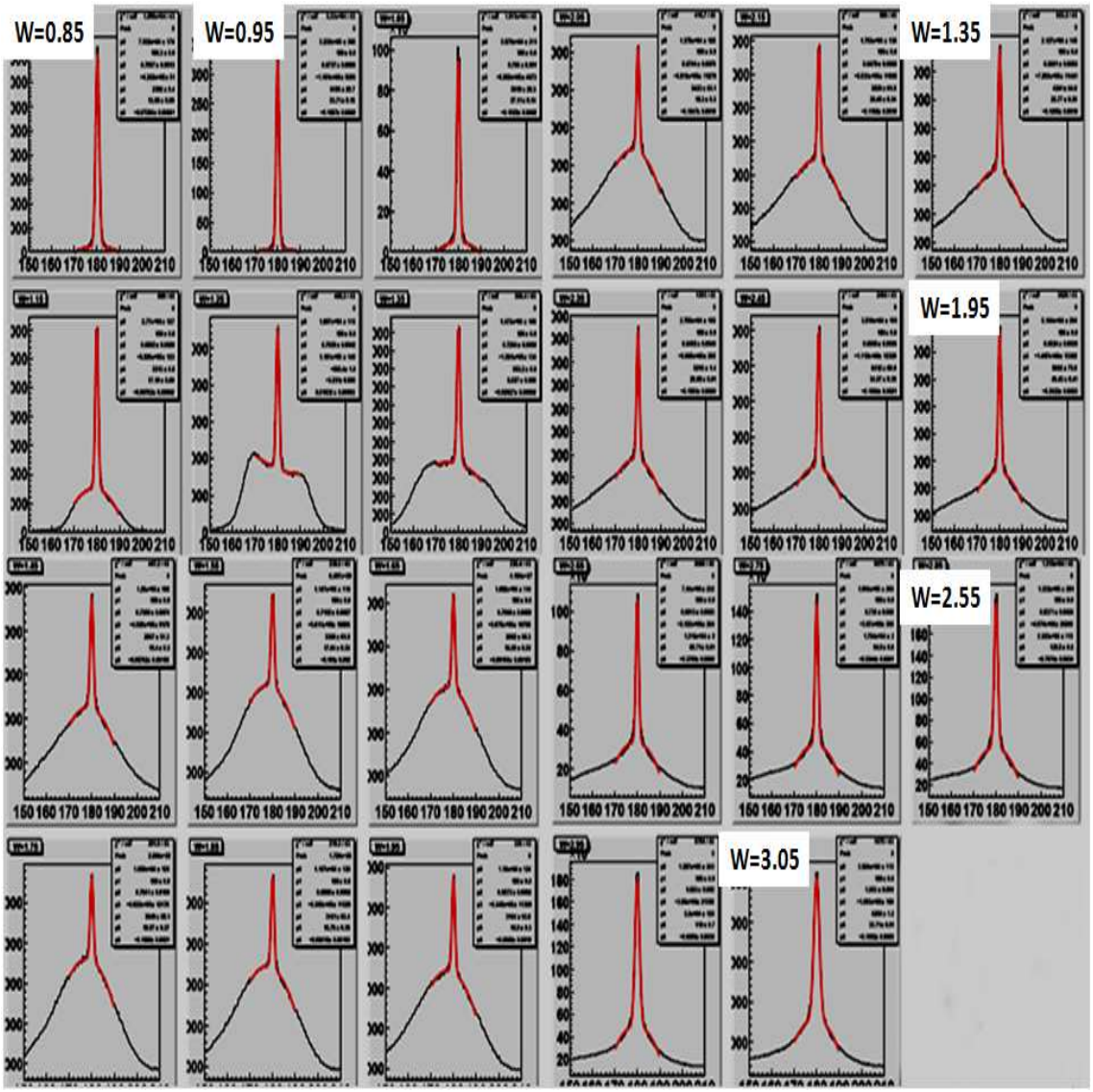

Figure 2: *Distributions of $\Delta\phi$ in 23 W-bins between 0.8 and 3.1 GeV, 0.1 GeV wide, with gauss plus polynomial fit (red lines).*

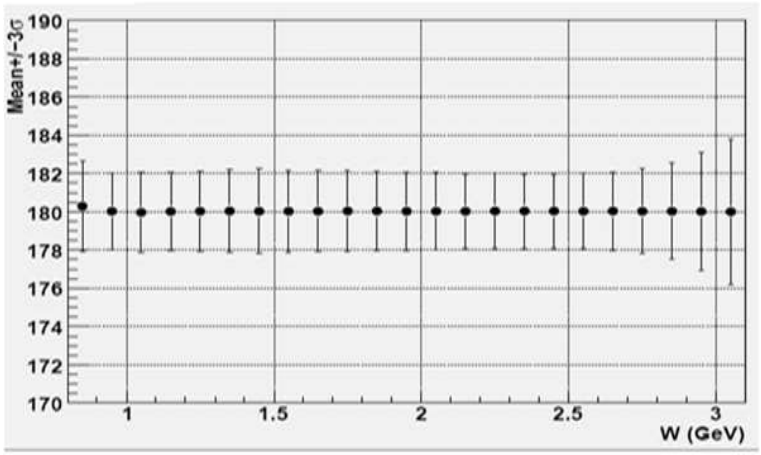

Figure 3: *Mean values of the fit of the $\Delta\phi$ distributions as a function of W (the error bars represent 3σ).*

2.2 Missing Mass cut

After the coplanarity cut, the missing mass squared distribution of the $ep \rightarrow e'pX$ has been plotted in the 23 bins of W (Fig. 4). For $W > 1.1$ GeV, each distribution has been fitted with a gaussian peak plus a second order polynomial. The mean values m from these fits are shown in Fig. 5, with the error bars representing 3 σ. The values of $m \pm 3\sigma$ have been fitted with a fourth order polynomial and the resulting curves used to select elastic (radiative or non radiative) events for $W > 1.1$ GeV. For lower W values no missing mass cuts have been applied.

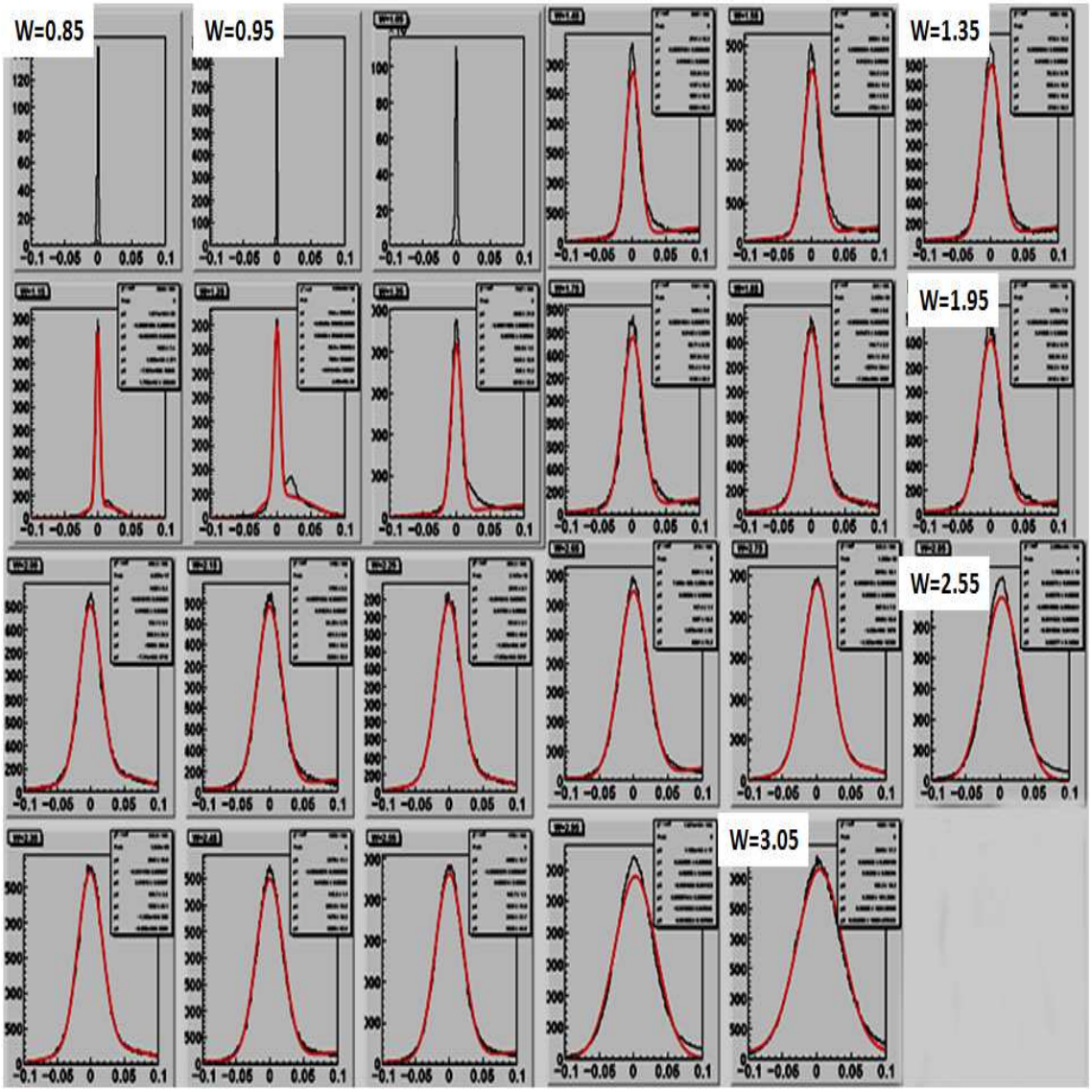

Figure 4: *Distributions of the e'pX missing mass squared in 23 W-bins between 0.8 and 3.1 GeV, 0.1 GeV wide, with gaussian fits (red lines).*

.

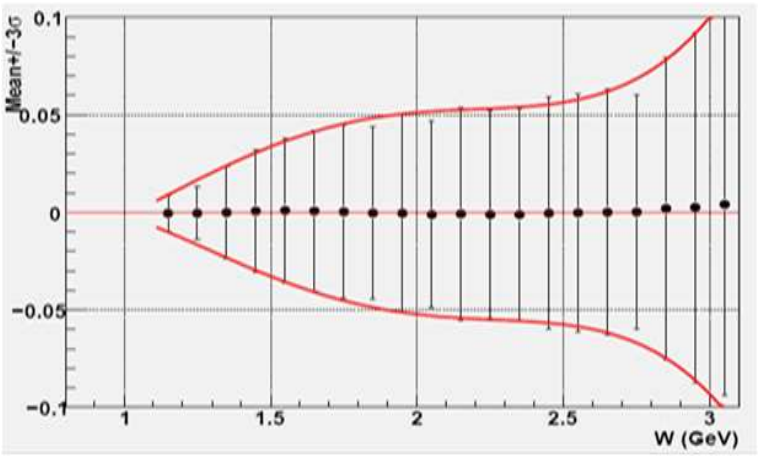

Figure 5: *Mean values of the fit of the e'pX missing mass squared distributions as a function of W (the error bars represent 3σ of the fit).*

3 Radiative event cuts

3.1 Initial state radiation

For non radiative events or when a photon is radiated by the incoming electron (Fig 1(a)), the proton angle can be calculated using the final electron energy E' and angle θ_e

$$\tan\theta_p^1 = \frac{M_p - E'(1-\cos\theta_e)}{M_p + E'\cos\theta_e}\frac{1}{\tan\frac{\theta_e}{2}} \tag{3}$$

The missing mass squared plotted versus

$$\Delta\theta_p^1 = \theta_p^{meas} - \theta_p^1 \tag{4}$$

shows two spots, one at $\Delta\theta_p^1 \approx 0$ corresponding to non radiative or initial radiation events, and a second one at negative $\Delta\theta_p^1$ corresponding to final radiation. An example of these distributions for the bin $W = 1.2 \div 1.3$ GeV is shown in fig. 6 (coplanarity cut only is applied here).

After applying missing mass cuts, the $\Delta\theta_p^1$ distributions have been fitted in 19 W bins (between 0.8 and 2.7 GeV, 0.1 GeV wide) with the sum of two gaussians plus a second order polynomial. The results are shown in Fig. 7. The obtained values of the mean m (with the error bars representing 3 σ) from the two fitted gaussians are shown in Fig. 8. The values of $m \pm 3\sigma$ in the figure have been fitted with a first (the values close to zero) and a third (the negative values) order polynomials to define the $\Delta\theta_p^1$ cuts.

3.2 Final state radiation

For non radiative events or when a photon is radiated by the detected electron (Fig 1(b)), the final proton angle can be calculated using the initial electron energy E and the final

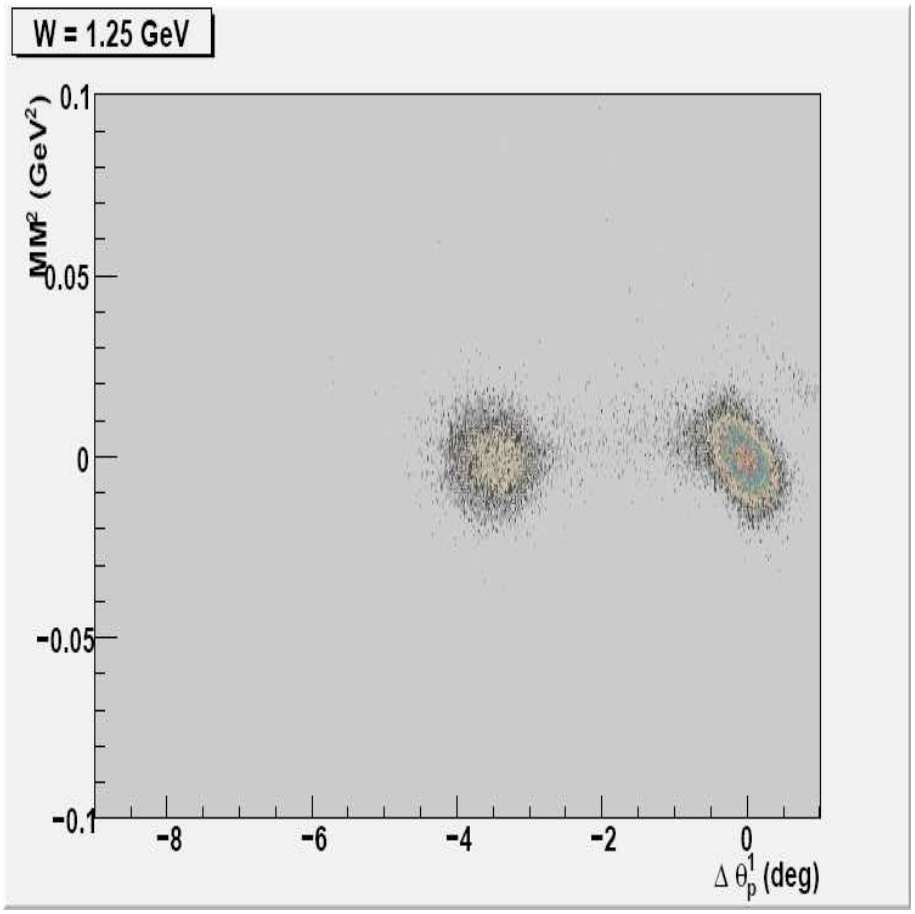

Figure 6: *Plot of the e'pX missing mass squared versus* $\Delta\theta_p^1$ *for* $W = 1.2 \div 1.3$ *GeV. Only coplanarity cut is applied here.*

electron angle (not affected by the radiation)

$$\tan\theta_p^2 = \frac{M_p}{M_p + E}\frac{1}{\tan\frac{\theta_e}{2}} \tag{5}$$

The missing mass squared plotted versus

$$\Delta\theta_p^2 = \theta_p^{meas} - \theta_p^2 \tag{6}$$

shows two spots, one at $\Delta\theta_p^2 \approx 0$ corresponding to non radiative or final radiation events, and a second one at positive $\Delta\theta_p^2$ corresponding to initial radiation. An example of these distributions for the bin $W = 1.2 \div 1.3$ GeV is shown in fig. 9 (coplanarity cut only is applied here).

After applying missing mass cuts, the $\Delta\theta_p^2$ distributions have been fitted in 19 W bins (between 0.8 and 2.7 GeV, 0.1 GeV wide) with the sum of two gaussians plus a second order polynomial. The results are shown in Fig. 10. The obtained values of the mean m (with the error bars representing 3 σ) from the two fitted gaussians are shown in Fig. 11.

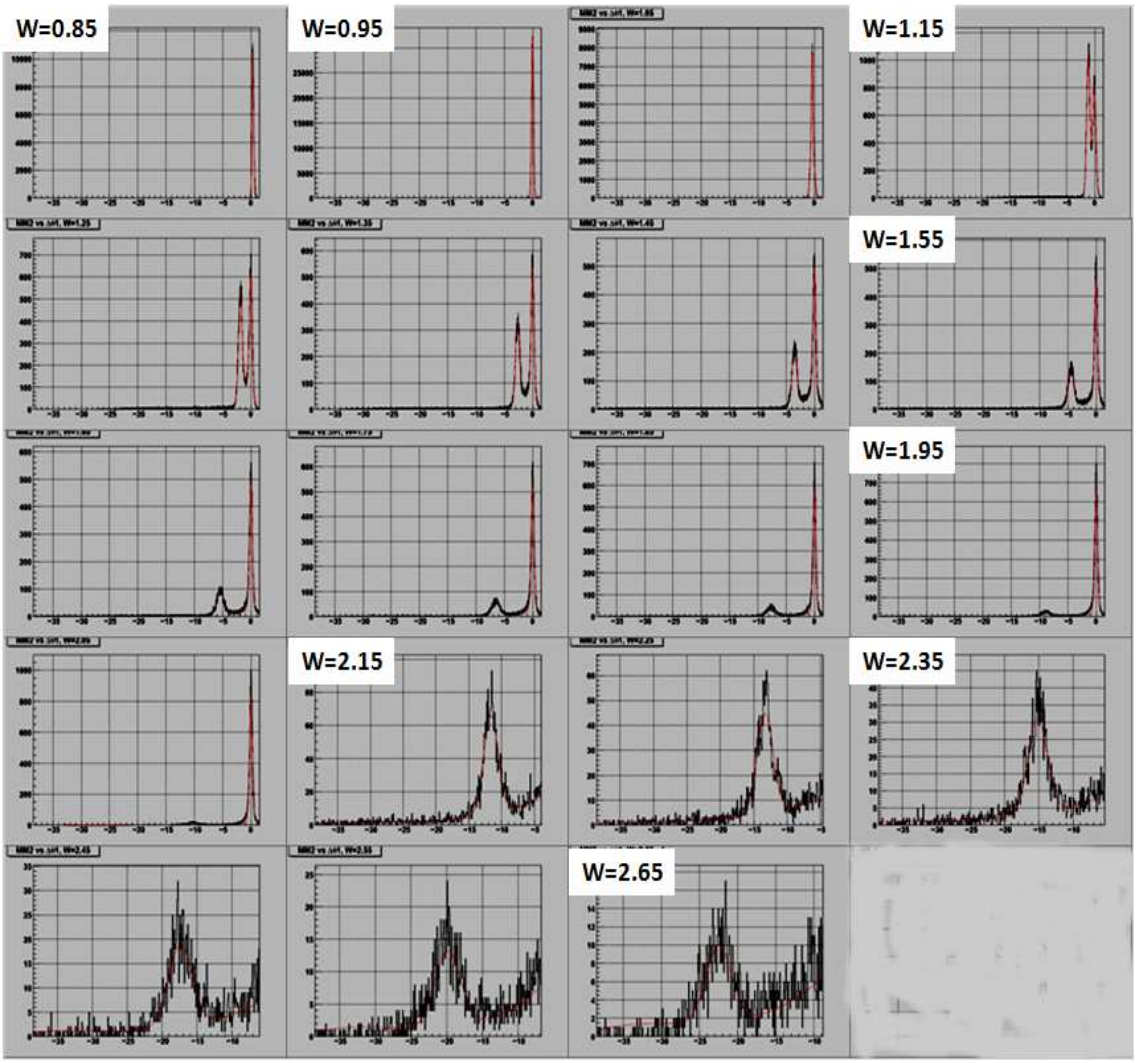

Figure 7: *Plots of the $\Delta\theta_p^1$ distributions in the 19 W bins between 0.8 2.7 GeV, 0.1 GeV wide. Note that for $W > 2.1$ GeV, only the first peak is shown.*

The values of $m \pm 3\sigma$ in the figure have been fitted with a first (the values close to zero) and a third (the negative values) order polynomials to define the $\Delta\theta_p^2$ cuts. Being the second peak very asymmetric with a large right tail, and being the background at large $\Delta\theta_p^2$ negligible, we used the second gaussian just to define the left edge of the peak.

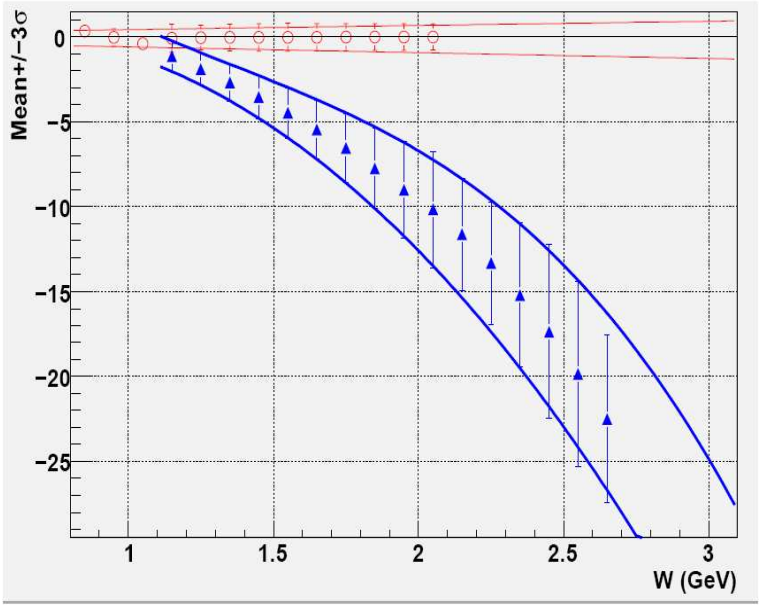

Figure 8: *Values of $m \pm 3\sigma$ of the two gaussians from the $\Delta\theta_p^1$ fits in Fig. 7 and their polynomial fits*

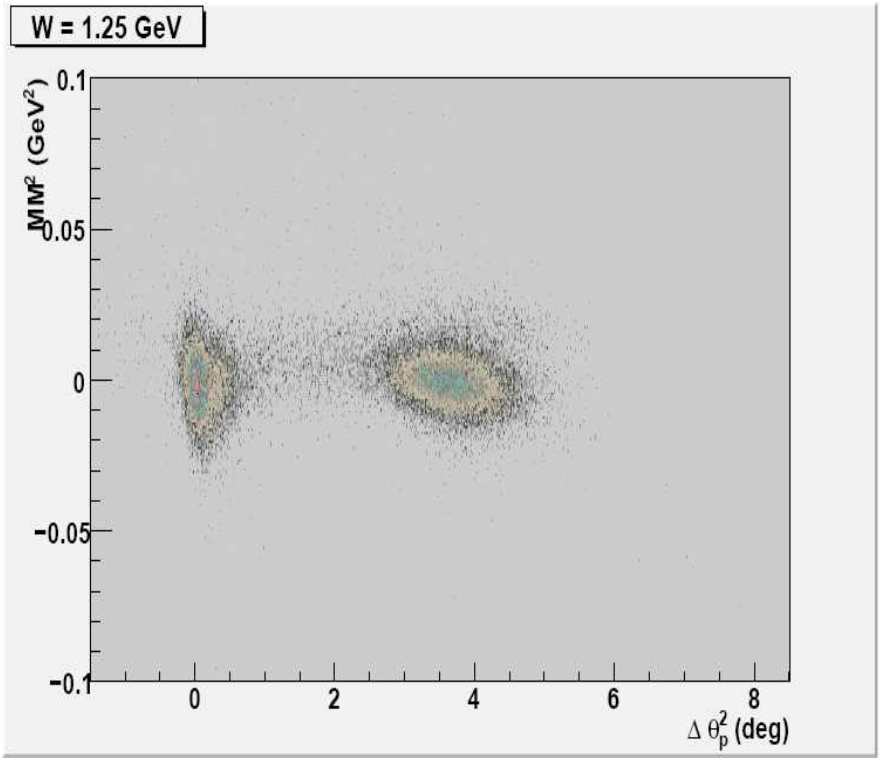

Figure 9: *Plot of the missing mass squared versus $\Delta\theta_p^2$ for $W = 1.2 \div 1.3$ GeV. Only coplanarity cut is applied here.*

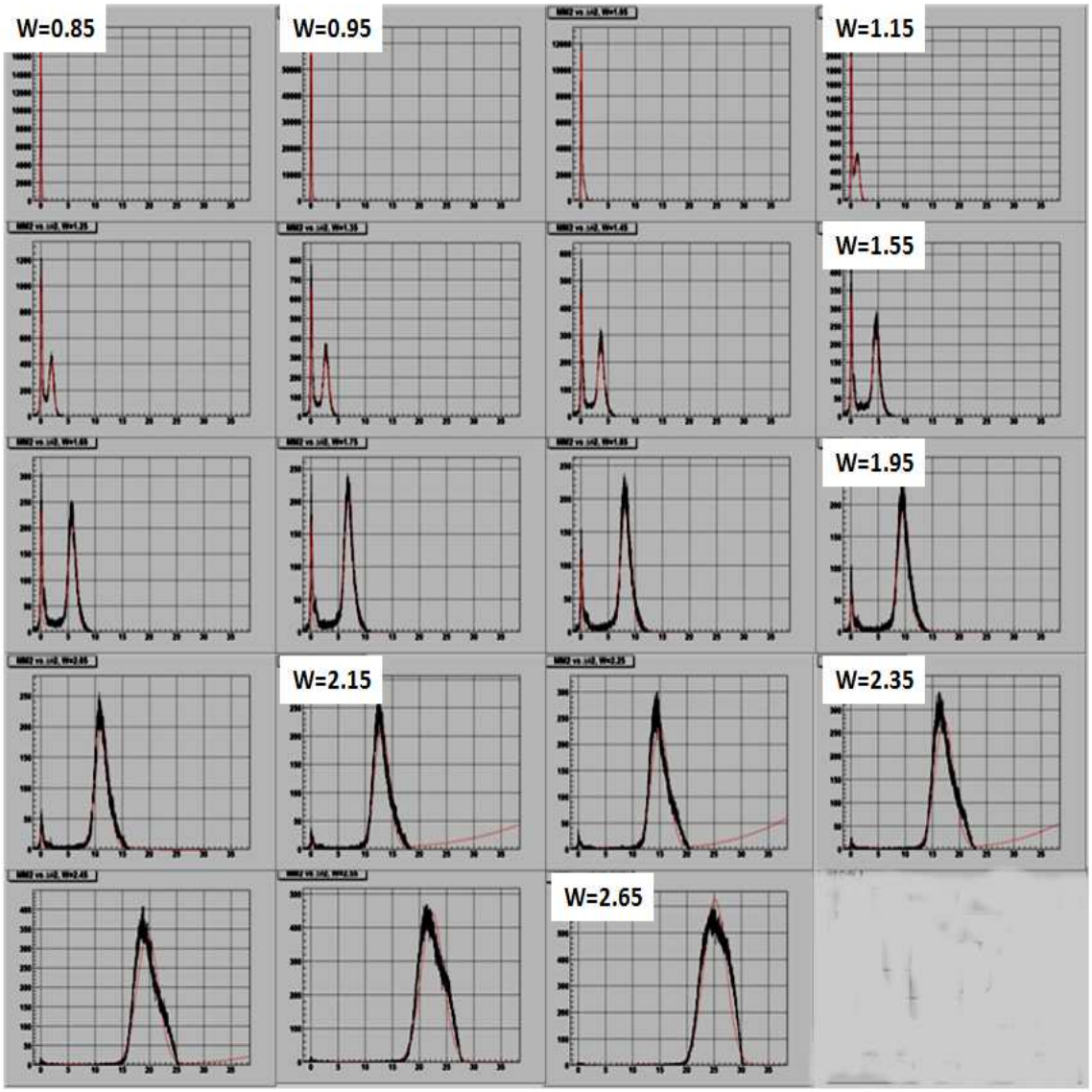

Figure 10: *Plots of the $\Delta\theta_p^2$ distributions in the 19 W bins between 0.8 2.7 GeV, 0.1 GeV wide. Note that for $W > 2.1$ GeV, only the first peak is shown.*

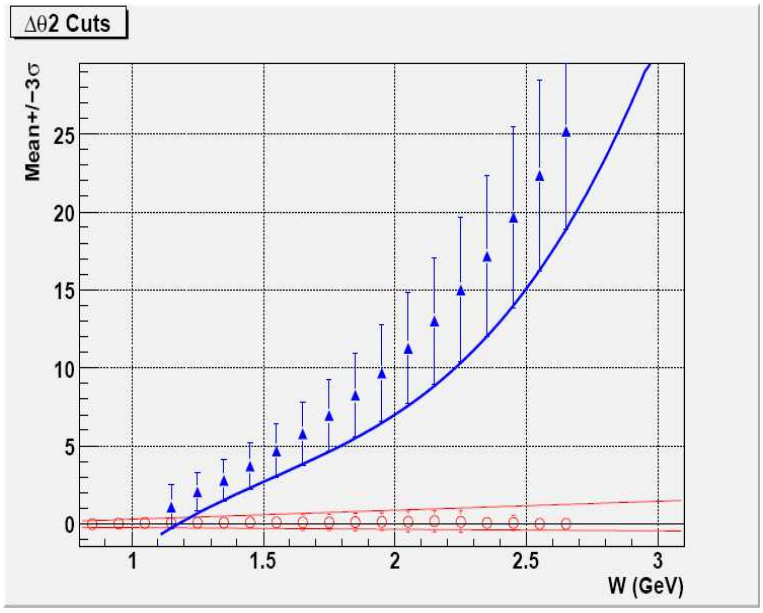

Figure 11: *Values of $m \pm 3\sigma$ of the two gaussians from the $\Delta\theta_p^2$ fits in Fig. 10 and their polynomial fits.*

3.3 Event selection

Elastic (radiative and non-radiative) events have been selected through the coplanarity and missing mass cuts. Event with no radiation are selected by $\Delta\theta_p^1, \Delta\theta_p^2 \approx 0$ (events between the two red lines in the Figs. 8 and 11). Initial state radiation events are selected by $\Delta\theta_p^1 \approx 0$ and $\Delta\theta_p^2 > 0$ (events between the two red lines in Fig. 8 and above the blue line in the Fig. 11, respectively). Final state radiation events are selected by $\Delta\theta_p^1 < 0$ and $\Delta\theta_p^2 \approx 0$ (events between the two blue lines in Fig. 11 and between the two red lines in the Fig. 8, respectively). Electron kinematic distributions for the three sets of events are shown in Fig. 12.

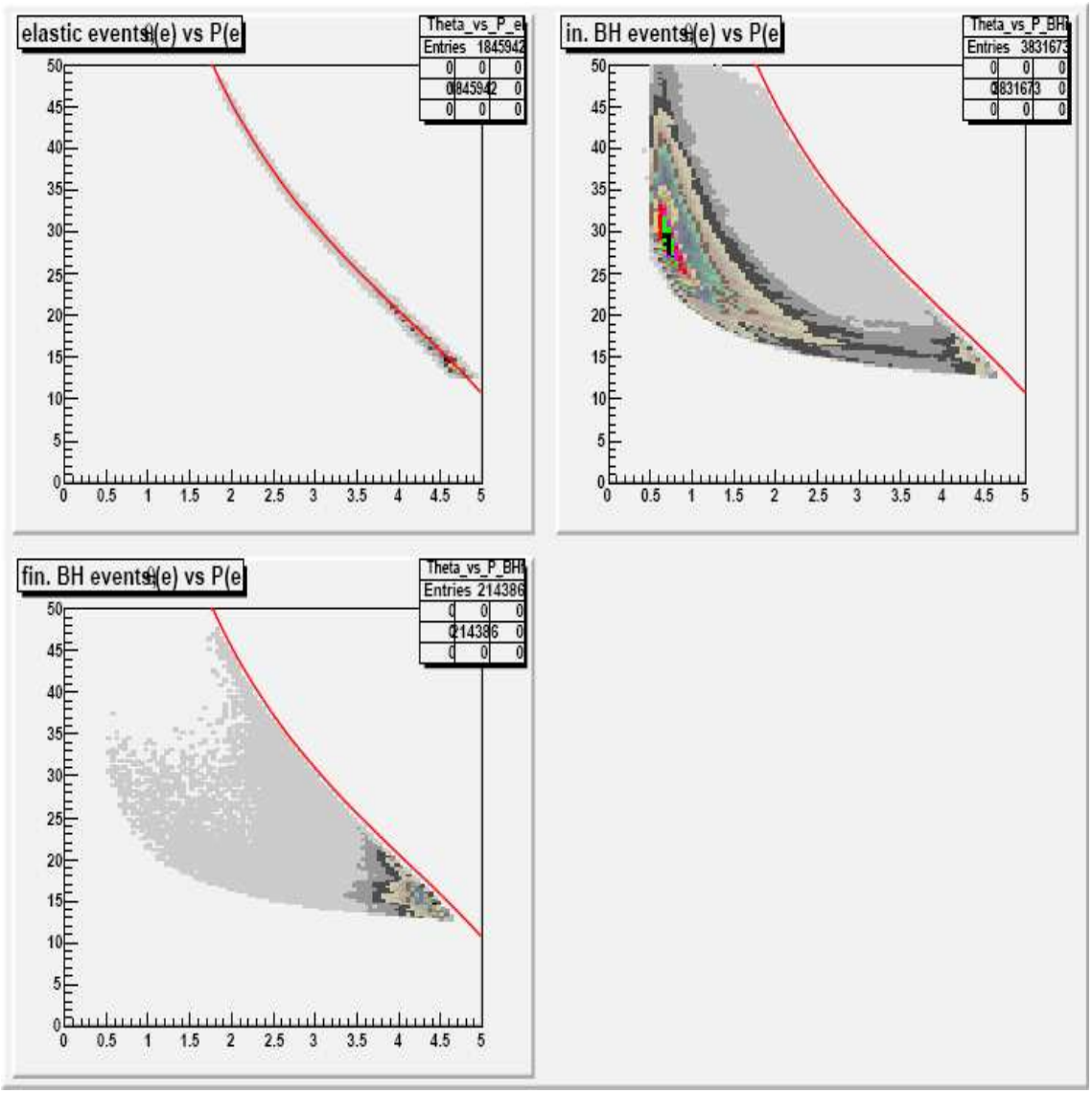

Figure 12: *Electron polar angle versus the momentum for elastic, initial and final state radiation events. The red line represent the theoretical curve for elastic events.*

4 Angle correction

Assuming that the measured angle distorsion comes from DC misalignment [1], the effect is the same for all the particles. Thus, one can calculate the angle correction for positive and negative particles from the same set of events. We use for this elastic (non radiative) events according to the cuts described in Sect. 3.

The calculation is done using eq. 5 with the measured electron beam energy $E = 5.49918$ GeV, solved as described in Fig. 13. Here, the full line represents eq. 5 and suppose that the point P represents the measured proton and electron angles. Calculating the mid distance points D and C of the measured angles from the theoretical curve along the horizontal and vertical axes, one obtain the first approximation corrected point P'. The procedure can be iterated starting now from point P' and determining a new approximated point P''. The iteration is stopped when the distance of the new point from the theoretical curve is less than 10^{-4}.

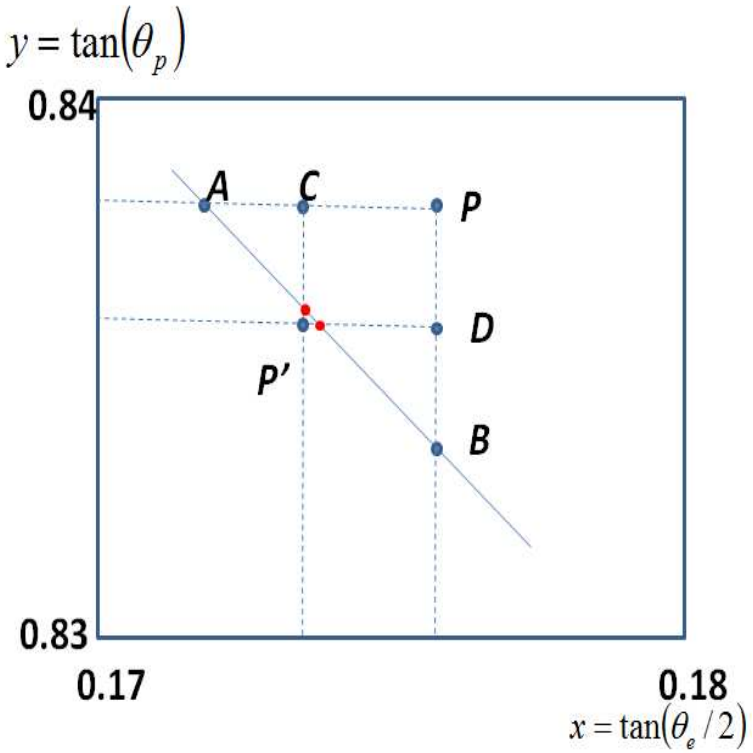

Figure 13: *Calculation of the angle correction (see text for details).*

The resulting corrections $\Delta\theta = \theta_{corr} - \theta_{meas}$ is very small, of the order of tenth of degree. Corrections from the electron and proton are combined together and plotted, sector by sector, in ϕ (3^o wide) and θ (1^o wide) bins. In each bin, the distribution of $\Delta\theta$ has been fitted with a gaussian curve. The means of the gaussian are plotted as a function of the azimuthal angle ϕ for few angular bins in sector 1 in Fig. 14. Bin-by-bin in θ, they have been fitted with a second order polynomial in ϕ. The parameters of these fits as a function of θ for sector 1 are shown as an example in Fig. 15.

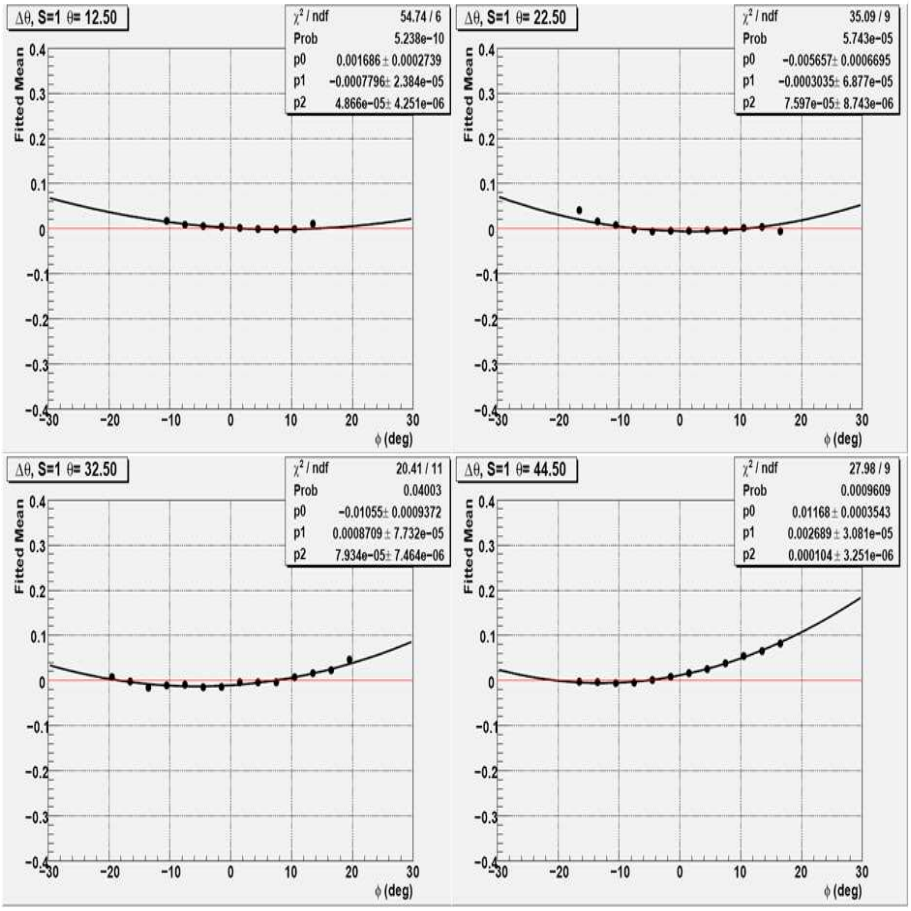

Figure 14: *Angular correction (in degrees) as a function of ϕ for 4 polar angle bins in sector 1.*

Thus, for each angular bin θ_i and for each sector s, the polar angle correction is given by

$$\Delta\theta(s, \theta_i, \phi) = c_0(s, \theta_i) + c_1(s, \theta_i)\phi + c_2(s, \theta_i)\phi^2 \tag{7}$$

and, for a given θ, an interpolation between two adjacent angular bins is performed.

The effect of the correction can be checked by recalculating the beam energy using eq. 5 with the actual electron and proton angles and plotting

$$\Delta E = E^{meas} - E^{calc} \tag{8}$$

as a function of ϕ. The results before and after the correction are shown in Fig. 16.

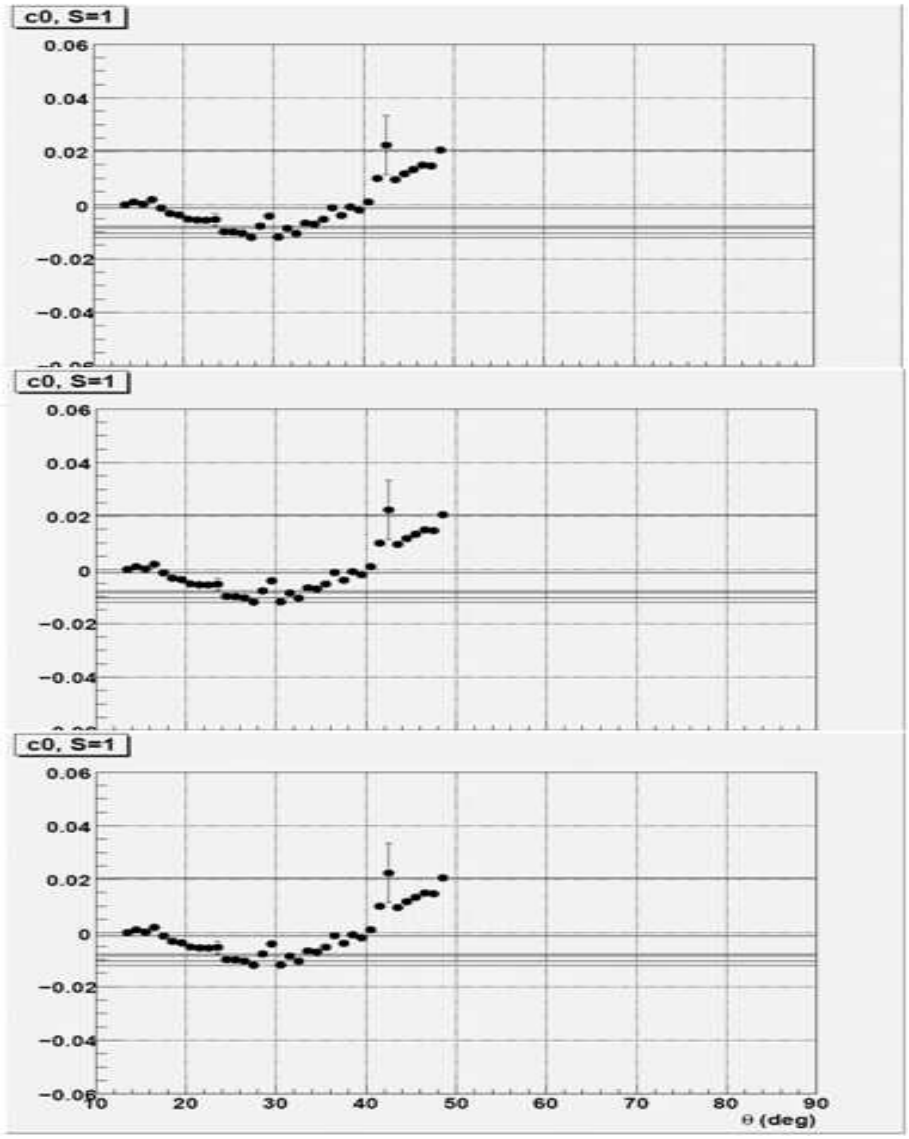

Figure 15: *Parameters of the second order polynomial fit of the ϕ dependence of the angular correction in sector 1.*

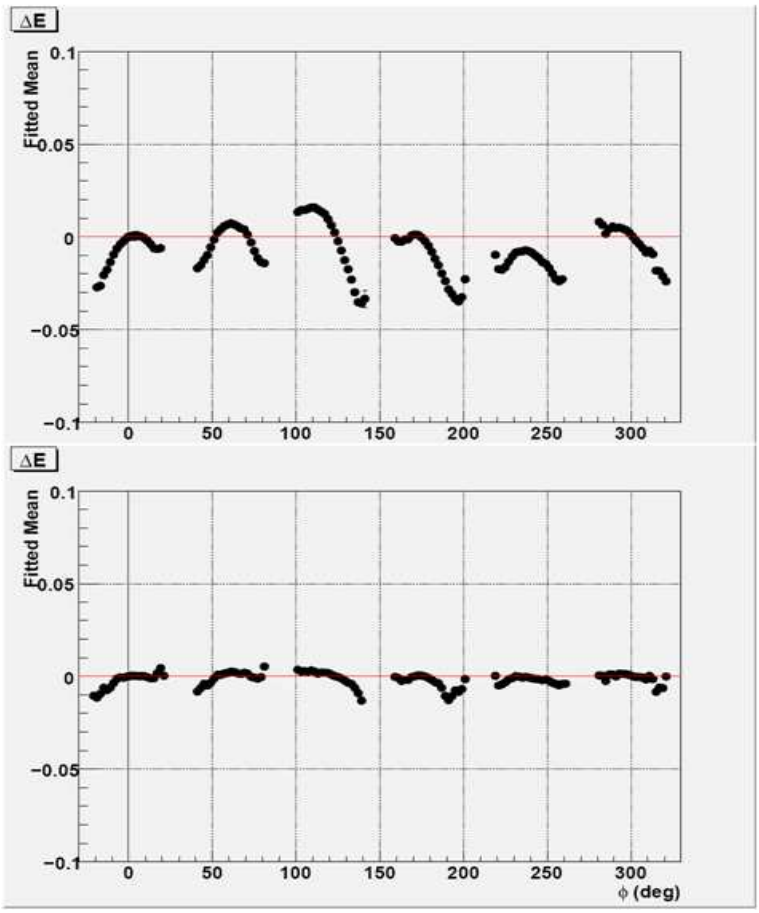

Figure 16: *ΔE as a function of ϕ before (upper plot) and after (lower plot) angle correction.*

5 Momentum correction for electrons

We now use elastic events together with those with initial state radiation. Final state radiation events cannot be used because the radiation changes the momentum of the detected electron.

5.1 Correction calculation

The corrected electron momentum can be computed from eq. 3

$$P_{corr} = M_p \frac{T-1}{1+(T-1)(1-cos(\theta_e)} \tag{9}$$

where $T = 1/[\tan(\theta_e/2)\tan(\theta_p)]$ and θ_e and θ_p are the corrected electron and proton polar angles. For the calculation, we selected elastic and initial state radiation events, cutting, as described in Sect. 3, $\Delta\theta_1$ and $\Delta\theta_2$ at the level of 5σ instead of 3σ as was done for the angle correction. This has been done because for some of the kinematic (angles and momentum) bins the 3σ limit (with the σ calculated by the W-dependence of the $\Delta\theta_1$ and $\Delta\theta_2$ distributions) can cut part of the $\Delta P = P_{corr} - P_{meas}$ distribution, as shown for example fone bin in Fig. 17.

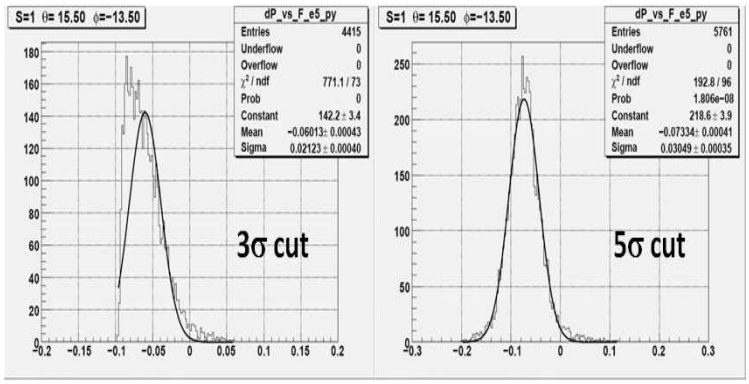

Figure 17: *ΔP distribution for one kinematic bin with 3 (left) or 5 (rigth) σ cut on $\Delta\theta_1$ and $\Delta\theta_2$ to select elastic events.*

The data have been binned in the sector, ϕ (4^o wide bins), θ (3^o wide bins) and, for the radiative events, P (0.2 GeV/c wide bins). The elastic events cover only one additional higher P bin for each angular bin. Each ΔP distribution has been fitted with a gaussian curve. For each sector, θ and P bin, the means of these curves have then been plotted as a function of ϕ, as shown for example in Fig. 18 for sector 1 and the angular bin $\theta = 14.5^o$. Bin-by-bin in P and θ, the ϕ dependence has been fitted with a linear curve, shown by the blue lines in the Figure.

The two parameters c_0 and c_1 of these linear fits have been plotted as a function of P for each sector and polar angle. Results for sector 1 are shown in Fig. 19. In each θ bin, the highest momentum data point comes from the elastic events, while all the rest of

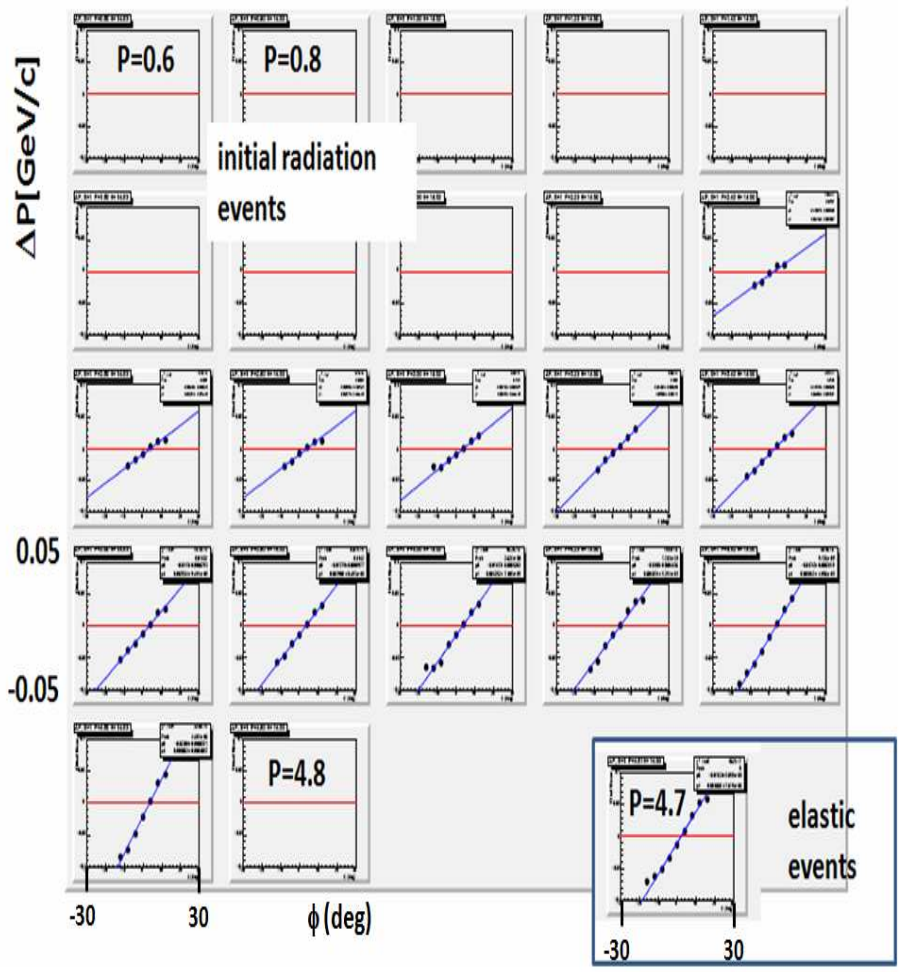

Figure 18: *Means of the gaussian fits of the ΔP distribution as a function of ϕ for all the momentum bins (sector 1, $\theta = 14.5^o$).*

the data points come from the radiative events. The momentum dependence of c_0 and c_1 has been finally fitted with polynomials of decreasing order from third (forward angles) to first (larger angles) as shown by the blue lines in Fig. 19.

The final momentum correction for each angular bin θ_i and for each sector s is given by

$$\Delta P(s, \theta_i, \phi, P) = c_0(s, \theta_i, P) + c_1(s, \theta_i, P)\phi \tag{10}$$

where for $j = 0, 1$

$$c_j(s, \theta_i, P) = \sum_{n=0}^{n_{max}} a_n(s, \theta_i) P^n \tag{11}$$

Again, for a given θ, an interpolation between two adjacent angular bins is performed.

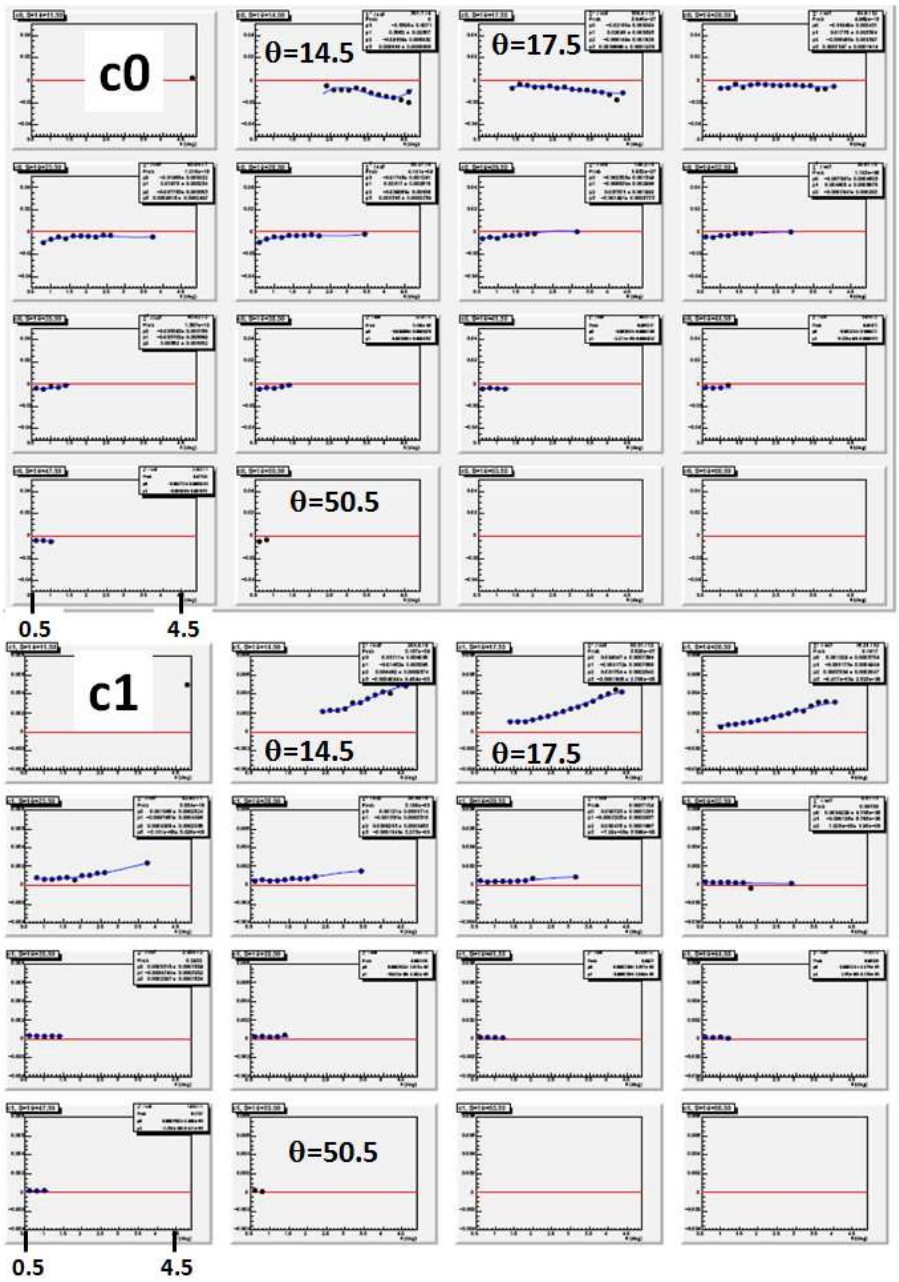

Figure 19: *Parameters c_0 (upper part) and c_1 (lower part) of the ϕ dependence of the momentum correction as a function of P for sector 1 in each θ bin.*

5.2 Results for electrons

To check the obtained electron momentum correction, the following reactions have been studied:

- $ep \to e'X$ looking for the missing elastic proton peak;
- $ep \to e'\pi^+X$ looking for the missing neutron peak;
- $ep \to e'K^+X$ looking for the missing Λ peak;
- $ep \to e'\pi^+\pi^-X$ looking for the missing proton peak;
- $ep \to e'p\pi^-X$ looking for the missing π^+ peak.

For each of these reactions, the missing mass squared has been plotted and fitted with a gaussian plus a polynomial background in several kinematic binning.

The Figs. 20 and 21 show the mean and σ of the squared missing mass distributions in $ep \to e'X$ events as a function of θ for the six sectors. The black empty squares are the results before the corrections, the red full circles after the corrections. The red lines in Fig. 20 represent the squared proton mass. As can be seen, the corrections really improve the results, small residual dependencies, in particular for sector 3, remain only for the larger θ angles.

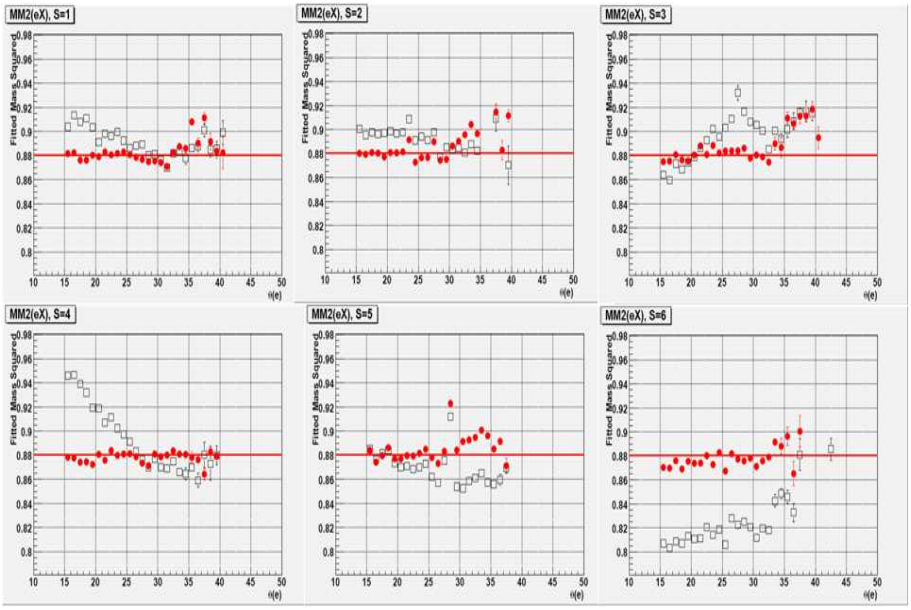

Figure 20: *Means of $MM^2(ep \to e'X)$ as a function of the electron angle for the six sectors (top left is sector 1, bottom right is sector 6). Black empty squares: before correction; red full circles: after electron corrections.*

The Figs. 22 and 23 show the mean and σ of the squared missing mass distributions as a function of the electron angles in sector 1 for the other four reactions in the list.

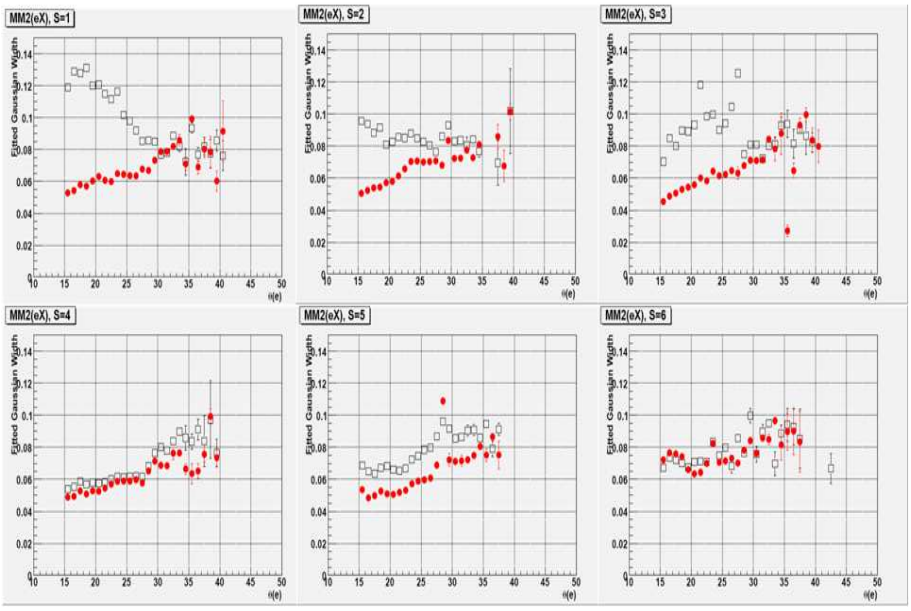

Figure 21: *Values of the σ of of $MM^2(ep \to e'X)$ as a function of the electron angle for the six sectors (top left is sector 1, bottom right is sector 6). Black empty squares: before correction; red full circles: after electron corrections.*

Similar results have been obtained for the other five sectors. These plots demonstrate that the correction works well also for electrons in non elastic events.

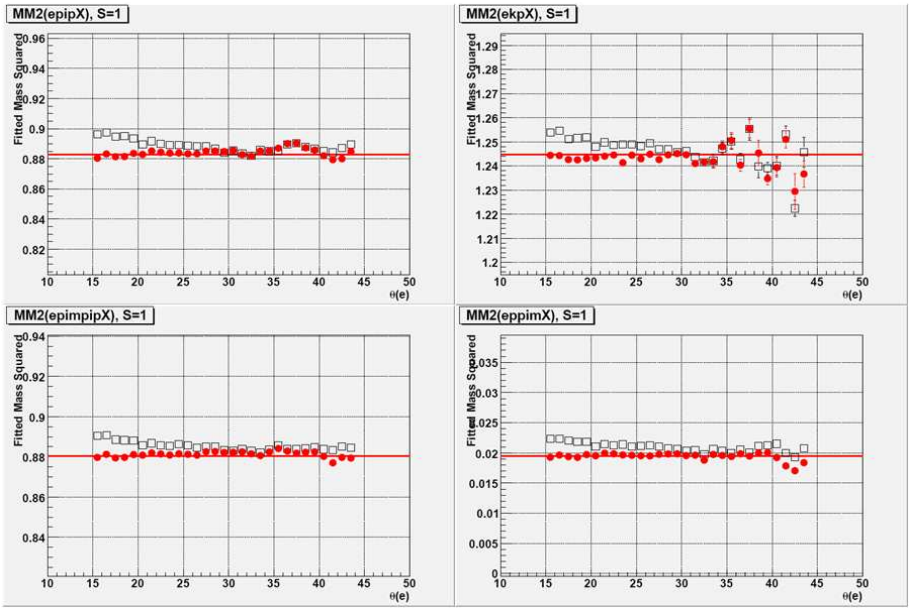

Figure 22: *From top right to bottom left: mean of* $MM^2(ep \to e'\pi^+X)$, $MM^2(ep \to e'K^+X)$, $MM^2(ep \to e'\pi^+\pi^-X)$, $MM^2(ep \to e'p\pi^-X)$ *as a function of the electron angle in sector 1. Black empty squares: before correction; red full circles: after electron corrections.*

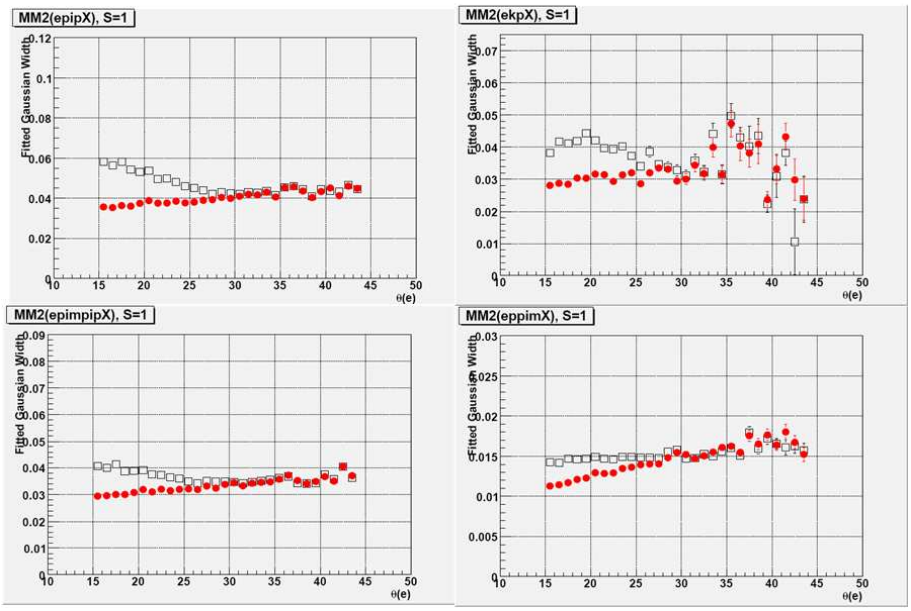

Figure 23: *From top right to bottom left:* σ *of* $MM^2(ep \to e'\pi^+X)$, $MM^2(ep \to e'K^+X)$, $MM^2(ep \to e'\pi^+\pi^-X)$, $MM^2(ep \to e'p\pi^-X)$ *as a function of the electron angle in sector 1. Black empty squares: before correction; red full circles: after electron corrections.*

5.3 Results for other negative particles

In Fig. 24, the kinematic distributions of θvsP for the π^- in the $ep \to e'p\pi^-X$ (top left) and $ep \to e'\pi^+\pi^-X$ (top right) is compared with that of electrons used to calculate the momentum correction. As can be seen, for angles below $\approx 50^o$, the distributions cover close regions in the kinematic plane, thus we can try to apply the calculated electron correction also to π^-. No correction is applied for larger angles.

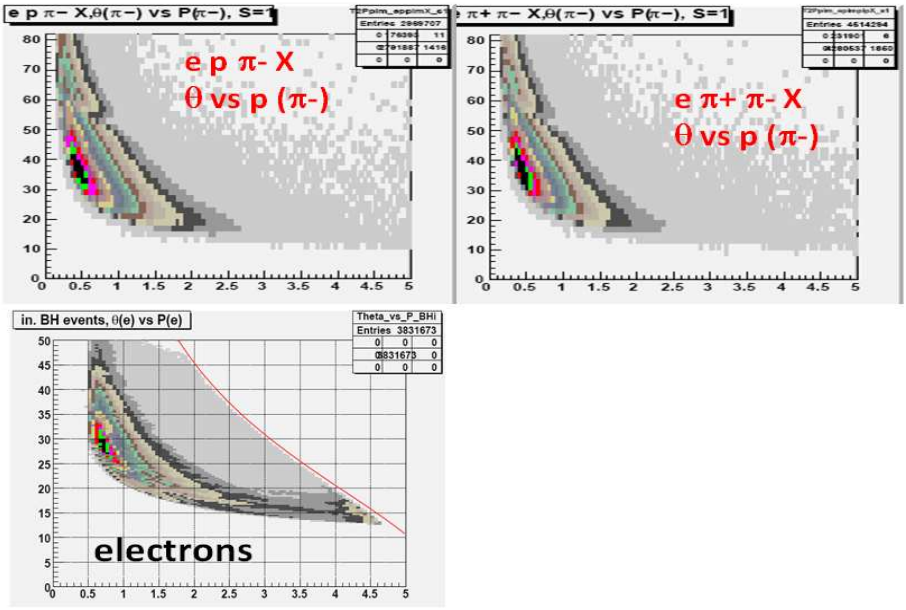

Figure 24: *Kinematic distribution θvsP for π^- in $ep \to e'p\pi^-X$ (top left) and $ep \to e'\pi^+\pi^-X$ (top right) and for electrons in initial state radiation Bethe-Heitler events.*

Results for the squared missing mass of $ep \to e'p\pi^-X$ and $ep \to e'\pi^+\pi^-X$ are shown in Fig. 25 as a function of π^- momentum for sector 1, 4 and 6. Black empty squares are results with no correction, blue empty triangles after electron correction and red full circles after electron and π^- correction. As can be seen, the correction reasonably take into account also residual dependencies due to π^- momentum error measurement. We therefore use this correction for **all** negative particles, even if the results for negative particles heavier than pion should be checked.

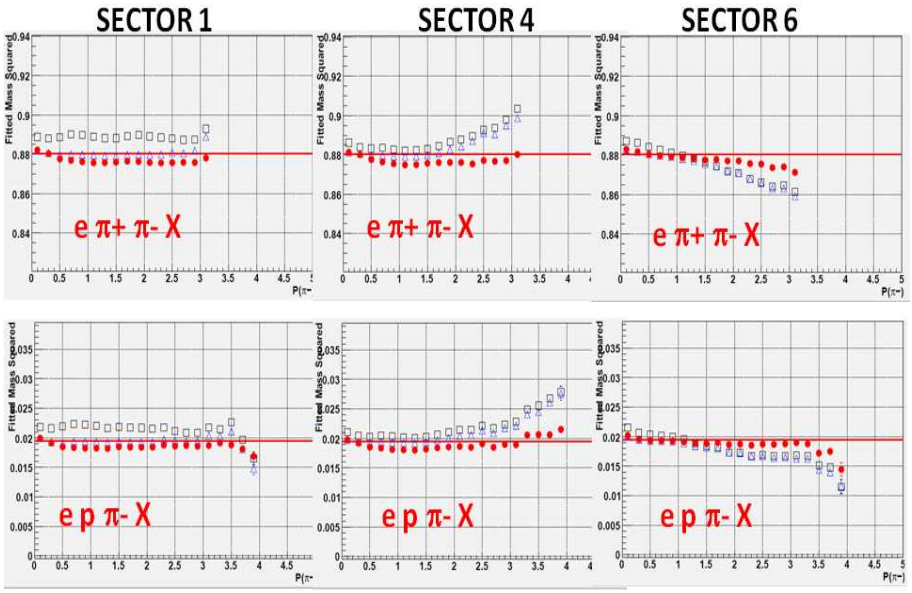

Figure 25: *Mean of* $MM^2(ep \to e'\pi^+\pi^- X)$ *(first row) and* $MM^2(ep \to e'p\pi^- X)$ *(second row) as a function of the* π^- *momentum in sector 1, 4 and 6. Black empty squares: before correction; blue empty triangles: after electron correction; red full circles: after electron and* π^- *corrections.*

6 Momentum correction for positive hadrons

Elastic protons (with or without radiation) are in general produced at large angles, thus the kinematic coverage they can provide is too limited. This is shown in Fig. 26, where the plot of θvsP for the elastic protons with initial state radiation is compared to the distributions for positive particles in other reactions. The largest kinematic coverage for a positive particle, together with the highest statistics, is provided by the $ep \to e'\pi^+X$ reaction. In addition, there is the advantage that only an one electron is also detected, for which the momentum corrections are well tested. We then used $ep \to e'\pi^+X$ events to calculate momentum corrections for positive hadrons.

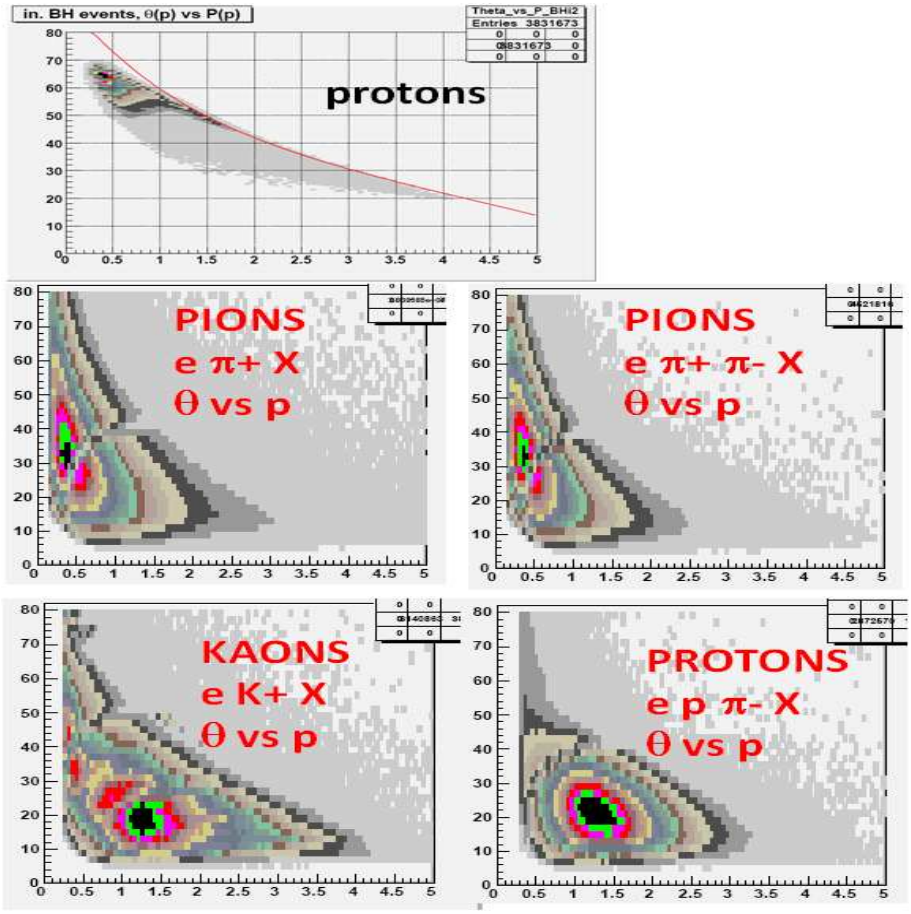

Figure 26: *Kinematic distributions θvsP for elastic protons (first plot), for π^+ in $ep \to e'\pi^+X$ and $ep \to e'\pi^+\pi^-X$ (second row), for kaons in $ep \to e'K^+X$ (third row, left) and for protons in $ep \to e'p\pi^-X$ (third row, right).*

6.1 Correction calculation

Events with one electron and one π^+ are selected. Electron 3-momentum correction and π^+ angle correction are applied. Energy loss correction [3] for the pion is also applied.

Then, exclusive events are selected by cutting on the squared missing mass. The Fig. 27 shows the mean values m of the squared missing mass distributions in 0.1 GeV wide W bins, with error bars representing 3σ and the straight red line representing the square of the neutron mass. The values of $m \pm 3\sigma$ have been fitted with a third order polynomial in W, shown in Fig. 27 by the red curves, which define the exclusive event cuts.

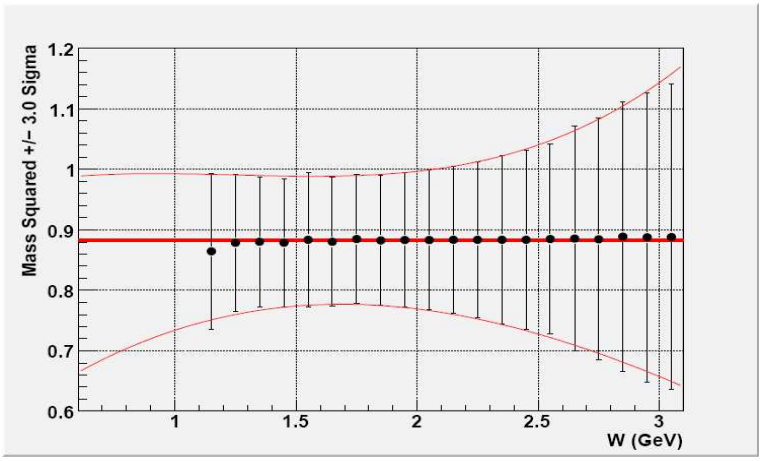

Figure 27: *Means (with error bars representing 3σ) of $MM^2(ep \to e'\pi^+X)$ as a function of W.*

The over-constrained kinematics of the $ep \to e'\pi^+n$ reaction allow now to calculate the corrected pion momentum using the known (corrected) angles of the electron and pion and the known (corrected) electron momentum

$$P_{corr} = \frac{A\sqrt{C^4 - m_\pi^2(A^2 - B^2)} + BC^2}{A^2 - B^2} \tag{12}$$

with m_π being the pion mass and A, B, C the kinematic quantities

- $A = E - E' + M_p$
- $B = E\cos\theta_\pi - E'\cos\theta_{e\pi}$
- $C^2 = \frac{M_p^2 + m_\pi^2 - M_n^2}{2} + M_p(E - E') - EE'(1 - \cos\theta_e)$

where $\theta_{e\pi}$ is the angle between the electron and the pion momenta. The procedure for the correction calculation follows that of Sect. 5. Distributions of the pion momentum correction $\Delta P = P_{corr} - P_{meas}$ have been computed for each sector of the pion and for ϕ (4^o wide), θ (3^o wide) and P (0.2 GeV/c wide) bins. Fits with a gaussian curve have been performed and the obtained means have been plotted as a function of ϕ for each sector and kinematical bin. Results for pions in sector 1 and the $\theta = 14.5^o$ bin are reported in Fig. 28 for all the momentum bins. The blue lines in the plots represent linear fits of the data points.

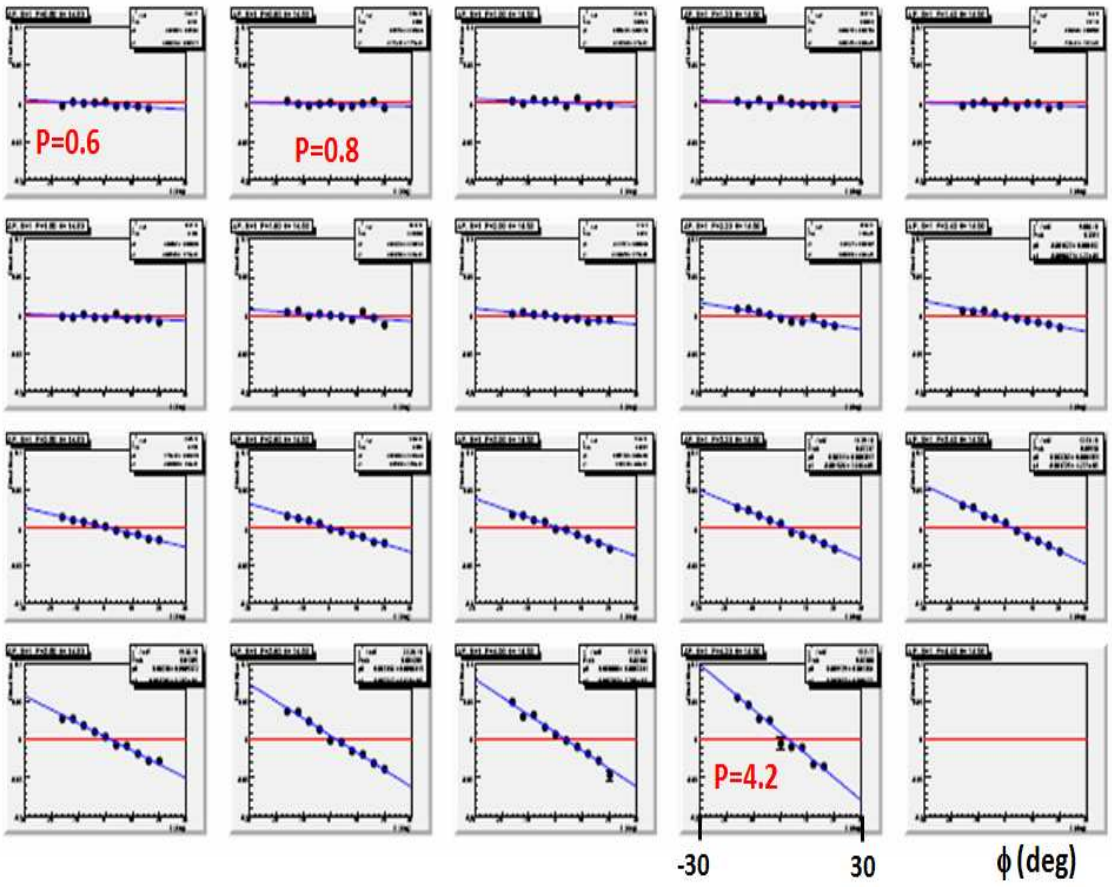

Figure 28: *Means of the gaussian fits of the pion ΔP distribution as a function of ϕ for all the momentum bins (sector 1, $\theta = 14.5^o$).*

The two parameters c_0 and c_1 of these linear fits have been plotted as a function of P for each sector and polar angle. Results for sector 1 are shown in Fig. 29. The momentum dependence of c_0 and c_1 has been finally fitted with polynomials of decreasing order from third (forward angles) to first (larger angles), as shown by the blue lines in Fig. 29.

The final π^+ correction has the same functional form (eq. 10 and 11) obtained for the electrons and also in this case interpolation between two adjacent θ bins is done.

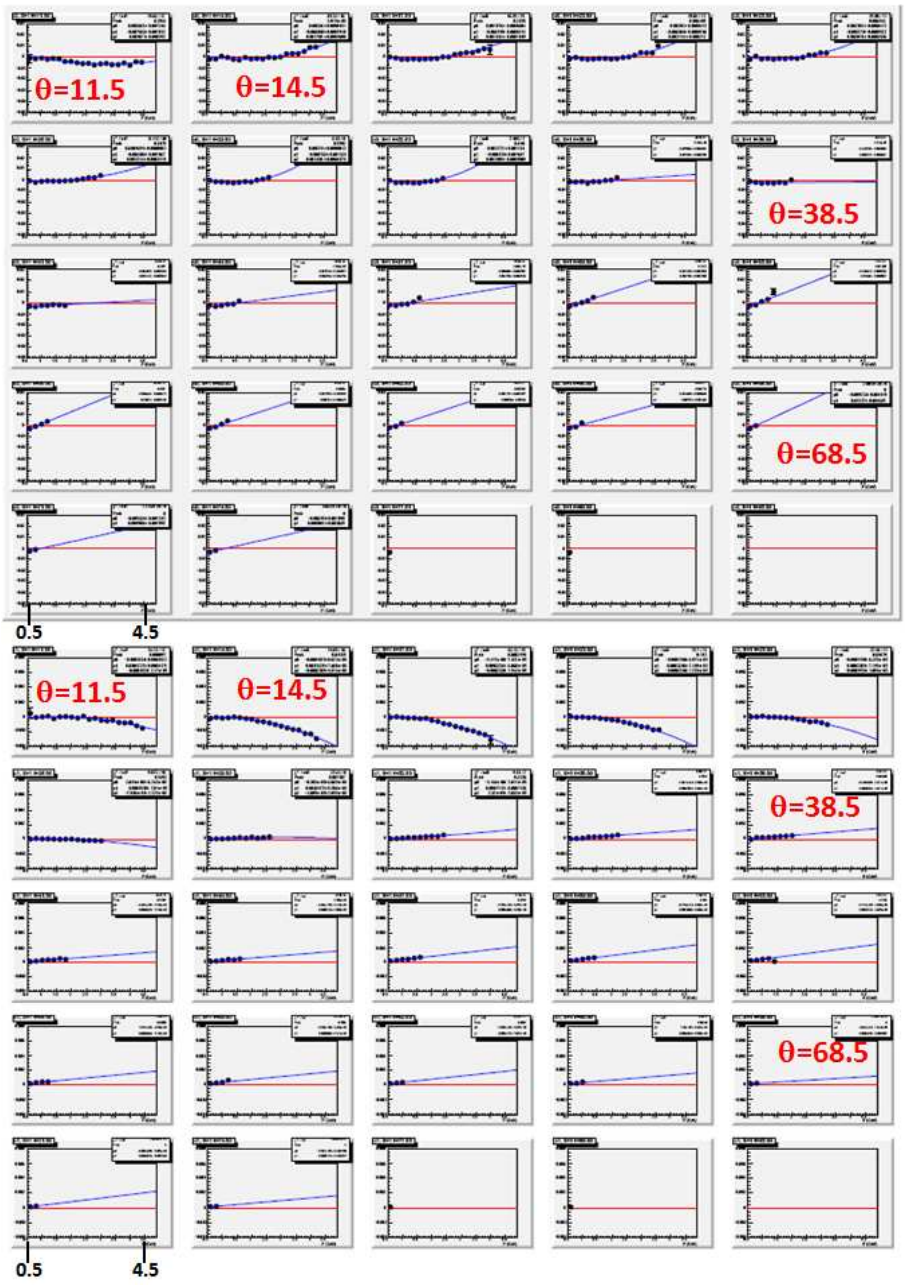

Figure 29: *Parameters c_0 (upper part) and c_1 (lower part) of the ϕ dependence of the momentum correction for sector 1 in each θ bin.*

6.2 Results for π^+

The mean and σ of the squared missing mass of $ep \to e'\pi^+X$ events are shown in the Figs. 30 and 31 for the six sectors as a function of the pion momentum. The black empty squares are the results before the corrections, the blue empty triangles results after electron correction and the red full circles after the electron and pion corrections. The red lines in Fig. 30 represent the squared neutron mass. As can be seen, the pion correction removes almost all the residual dependencies of the means and also improves the σ. Only small deviations at the highest pion momentum (i.e. more forward angles) survive.

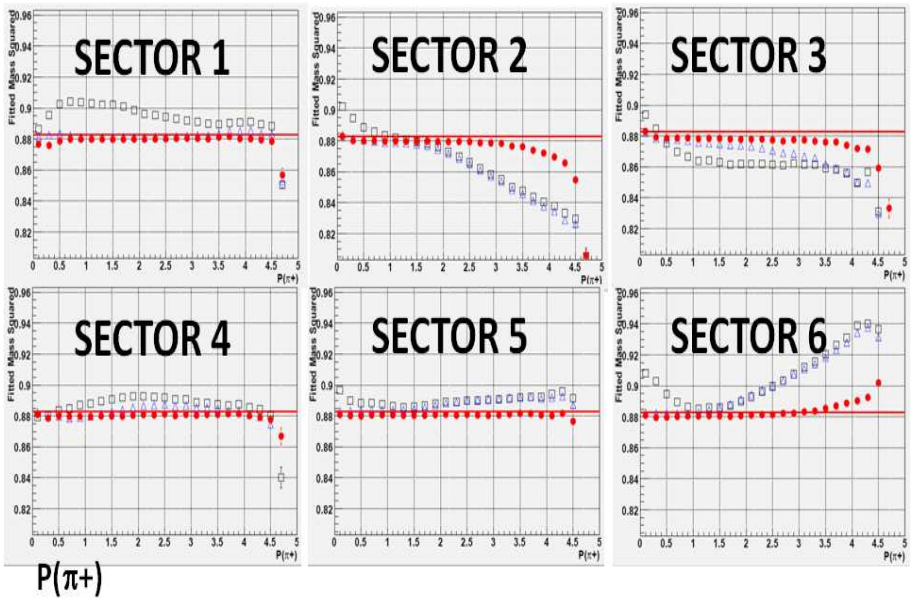

Figure 30: *Means of $MM^2(ep \to e'\pi^+X)$ as a function of the pion momentum for the six sectors. The black empty squares are the results before the corrections, the blue empty triangles results after electron correction and the red full circles after the electron and pion corrections.*

The results for the $ep \to e'\pi^+\pi^-X$ reaction are shown in Fig. 32 for sector 2, 3 and 6 (first row for the means, second row for the σ) as a function of the π^+ momentum. A good improvement has been found for these three sectors. The quality of the results for the other three sectors is similar, even if not a large improvement have been found, being the results already good after the electron correction only.

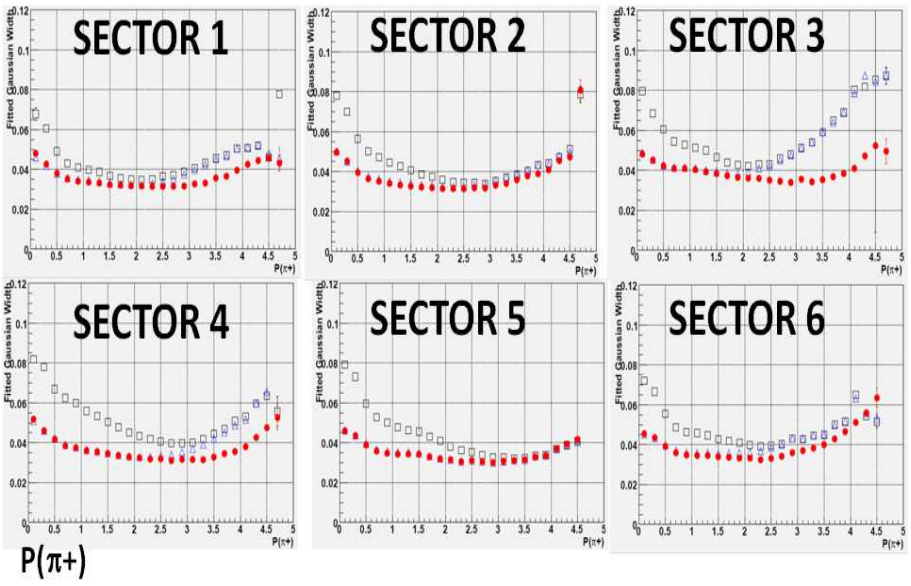

Figure 31: *Values of the σ of of $MM^2(ep \to e'\pi^+X)$ as a function of the pion momentum for the six sectors. The black empty squares are the results before the corrections, the blue empty triangles results after electron correction and the red full circles after the electron and pion corrections.*

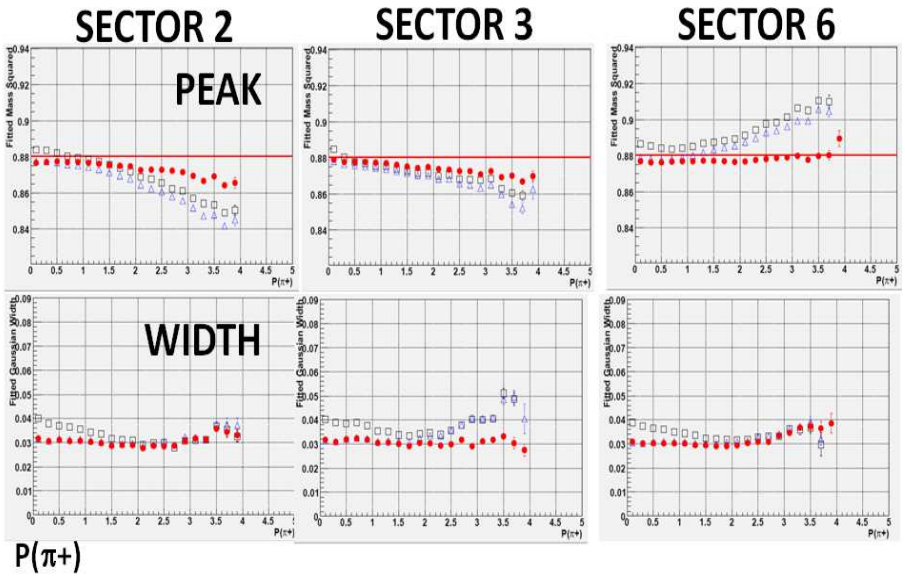

Figure 32: *Results for $MM^2(ep \to e'\pi^+\pi^-X)$ as a function of the π^+ momentum for the sector 2, 3 and 6: means (first row) and σ (second row). The black empty squares are the results before the corrections, the blue empty triangles results after electron correction and the red full circles after the electron and pion corrections.*

6.3 Results for other positive hadrons

The correction calculated for π^+ is now applied to other positive hadrons. In Fig. 33 the mean (first row) and σ (second row) of the $MM^2(ep \to e'p\pi^- X)$ distributions as a function of the proton momentum for sector 2, 3 and 6 are shown. The black empty squares are the results before the corrections, the blue empty triangles results after electron correction and the red full circles after the electron and proton corrections. The red lines in the plots of the means represent the squared pion mass. The same plots for the $MM^2(ep \to e'K^+X)$ are reported in Fig. 34, where the red lines represent now the squared Λ mass. Similar results have been found for the other three sectors. For both the reactions, the correction calculated for π^+ reasonably account for deviations in the proton and kaon momentum measurements too. The residual dependencies could be corrected only by implementing *ad hoc* corrections, that are beyond the scope of this note. We therefore use these corrections for **all** positive particles.

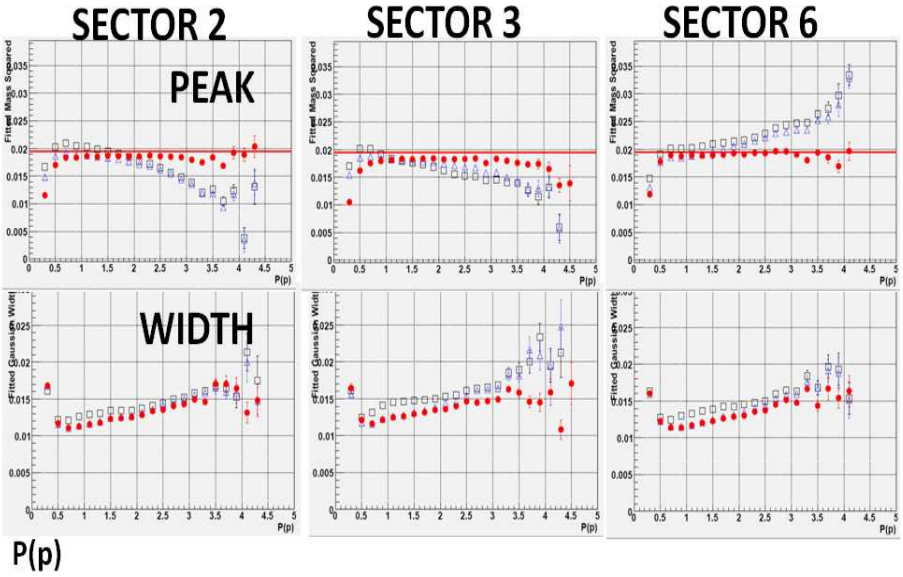

Figure 33: *Results for $MM^2(ep \to e'p\pi^- X)$ as a function of the proton momentum for the sector 2, 3 and 6: means (first row) and σ (second row). The black empty squares are the results before the corrections, the blue empty triangles results after electron correction and the red full circles after the electron and pion corrections.*

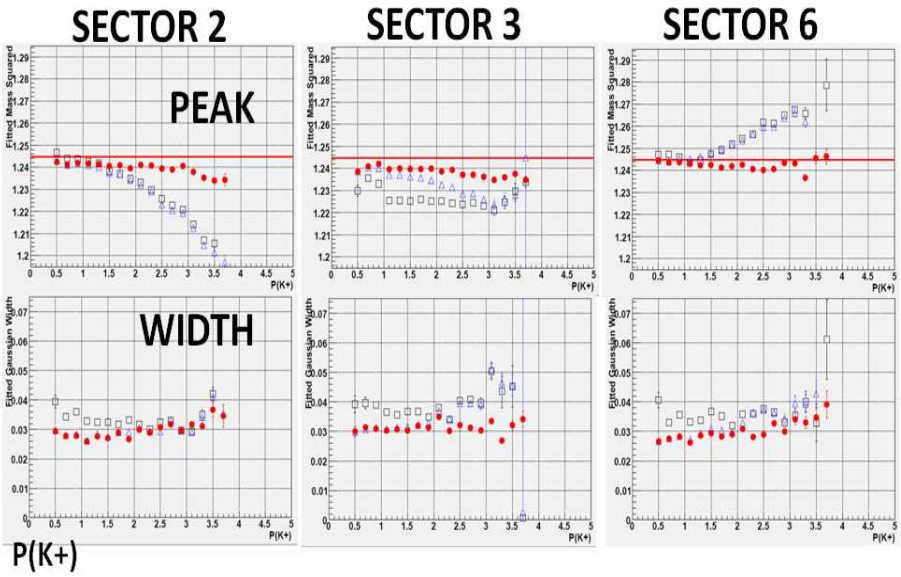

Figure 34: *Results for $MM^2(ep \to e'K^+X)$ as a function of the kaon momentum for the sector 2, 3 and 6: means (first row) and σ (second row). The black empty squares are the results before the corrections, the blue empty triangles results after electron correction and the red full circles after the electron and pion corrections.*

7 Invariant mass distributions

The obtained corrections have been demonstrated to work well in improving the resolution of missing mass distributions in several reactions. On the contrary, when looking at invariant mass distributions, these same corrections could produce slight worsening of the resolution. This has been found for example by looking at the Λ mass in $ep \to ep\pi^- X$ events, where correcting the proton and pion momenta produces an increase of the σ of the peak by about 15%. This is not a big issue, because invariant mass distributions have usually small widths (for example, the Λ peak has $\sigma \approx 1$ MeV). However, this effect must be taken into account to decide wether momentum corrections are necessary or not when studying invariant mass distributions.

8 Code for the correction

Code for using the whole momentum correction described in this note can be found in [4]. For Fortran users, the file *momcorr_f.tar* contains a set of the necessary routines. For C++ users, the file *MomCorr.C* contains the definition of a class performing the correction. A *readme.txt* file can also be found, explaining how to use the code. For both Fortran and C++, the input parameters for the calculation has been stored in the set of out files in [4].

9 Conclusions

The calculation of the 3-momentum correction for the $e1f$ data sets has been discussed in this note. The polar angle correction has been calculated using electrons and protons from elastic scattering. The electron momentum correction has been calculated using elastic and radiative ep events. This correction can be used for elastic as well non elastic reaction channels, improving both the peak and σ of the missing mass distributions. It has been found that the same correction works well also for π^-. Results for other negative hadrons should be tested. The momentum correction for π^+ has been calculated using $ep \to e'\pi^+(n)$ events. This correction works reasonably well also for other positive hadrons. Fortran and C++ routines have been implemented.

References

[1] M. Ungaro, http://www.jlab.org/ ungaro/maureepage/proj/pi0_Delta/docs/e1_prl.pdf

[2] Root files in the directory /mss/clas/e1f/production/pass2/v1/root/e/

[3] http://www.jlab.org/Hall-B/secure/e1f/mirazita/eloss/

[4] http://www.jlab.org/Hall-B/secure/e1f/mirazita/momcorr/